Nakahata S, Saito Y, Marutsuka K, Hidaka T, Maeda K, Hatakeyama K, Shiraga T, Goto A, Takamatsu N, Asada Y, Utsunomiya A, Okayama A, Kubuki Y, Shimoda K, Ukai Y, Kuosawa G, Morishita K.	Clinical significance of CADM1/TSLC1/IgSF4 expression in adult T-cell leukemia/ lymphoma.	Leukemia	26(6)	1238-46	2012
Kanda J, Hishizawa M, Utsunomiya A, Taniguchi S, Eto T, Moriuchi Y, Tanosaki R, Kawano F, Miyazaki Y, Masuda M, Nagafuji K, Hara M, Takanashi M, Kai S, Atsuta Y, Suzuki R, Kawase T, Matsuo K, Nagamura-Inoue T, Kato S, Sakamaki H, Morishima Y, Okamura J, Ichinohe T, Uchiyama T.	Impact of graft-versus-host disease on outcomes after allogeneic hematopoietic cell transplantation for adult T-cell leukemia: a retrospective cohort study.	Blood	119(9)	2141-48	2012
Gupta A, Nuber N, Esslinger C, Wittenbrink M, Treder M, Landshammer A, Noguchi T, Kelly M, Gnjatic S, Ritter E, von Boehmer L, Nishikawa H, Shiku H, Old LJ, Ritter G, Knuth A, van den Broek M.	A novel human-derived monoclonal antibody against NY-ESO-1 improves the efficacy of chemotherapy.	Cancer Immunity	13	E3	2013
Eikawa S, Kakimi K, Isobe M, Kuzushima K, Luescher I, Ohue Y, Ikeuchi K, Uenaka A, Nishikawa H, Udono H, Oka M, Nakayama E.	Induction of CD8 T-cell responses restricted to multiple HLA class I alleles in a cancer patient by immunization with a 20-mer NY-ESO-1f (NY-ESO-1 91-110) peptide.	International Journal of Cancer	132	345-54	2013

2013

発表者氏名	論文タイトル名	発表誌名	巻号	ページ	出版年
Ishida T, Ito A, Sato F, Kusumoto S, Iida S, Inagaki H, Morita A, Akinaga S, Ueda R.	Stevens-Johnson Syndrome associated with mogamulizumab treatment of Adult T-cell leukemia/lymphoma.	Cancer Sci.	104	647-50	2013
Ogura M*, Ishida T*, Hatake K, Taniwaki M, Ando K, Tobinai K, Fujimoto K, Yamamoto K, Miyamoto T, Uike N, Tanimoto M, Tsukasaki K, Ishizawa K, Suzumiya J, Inagaki H, Tamura K, Akinaga S, Tomonaga M, Ueda R.	Multicenter phase II study of mogamulizumab (KW-0761), a defucosylated anti-CCR4 antibody, in patients with relapsed peripheral T-cell lymphoma and cutaneous T-cell lymphoma.	J Clin Oncol,	in press.		
Narita T, Ishida T, Masaki A, Suzuki S, Ito A, Mori F, Yamada T, Masaki Ri, Kusumoto S, Komatsu H, Miyazaki Y, Takatsuka Y, Utsunomiya A, Niimi A, Iida S, Ueda R.	HTLV-1 bZIP factor specific CD4 T cell responses in ATL patients after allogeneic hematopoietic stem cell transplantation.	J Immunol.	192 (3)	940-7	2014
Ishida T, Hishizawa M, Kato K, Tanosaki R, Fukuda T, Takatsuka Y, Eto T, Miyazaki Y, Hidaka M, Uike N, Miyamoto T, Tsudo M, Sakamaki H, Morishima Y, Suzuki R, Utsunomiya A, et al.	Impact of GVHD on allogeneic hematopoietic cell transplantation for adult T-cell leukemia-lymphoma focusing on preconditioning regimens: nationwide retrospective study Biology of Blood and Marrow Transplantation.	Biol Blood Marrow Transplant.	19	1731-9	2013
Suzuki T, Kusumoto S, Yoshida T, Mori F, Ito A, Ri M, Ishida T, Komatsu H, Niimi A, Iida S.	Successful salvage therapy using lenalidomide in a patient with relapsed multiple myeloma after allogeneic hematopoietic stem cell transplantation.	Int J Hematol.	97	540-3	2013

Xia H, Yamada S, Aoyama M, Sato F, Masaki A, Ge Y, Ri M, Ishida T, Ueda R, Utsunomiya A, Asai K, Inagaki H.	Prognostic impact of miR-145 down-regulation in adult T-cell leukemia/ lymphoma.	Hum Pathol.	in press		
Masaki A, Ishida T, Suzuki S, Ito A, Mori F, Sato F, Narita T, Yamada T, Ri M, Kusumoto S, Komatsu H, Tanaka Y, Niimi A, Inagaki H, Iida S, Ueda R.	Autologous Tax-specific CTL therapy in a primary ATL cell-bearing NOD/Shi-scid, IL-2Rγnull mouse model.	J Immunol.	191(1)	135-44	2013
Sato F ,Ishida T, Ito A, Mori F, Masaki A, Takino H, Narita T, Ri M, Kusumoto S, Suzuki S, Komatsu H, Niimi A, Ueda R, Inagaki H, Iida S.	Angioimmunoblastic T-cell lymphoma mice model.	Leuk Res.	37	21-7	2013
Inagaki A, Tajima E, Uranishi M, Totani H, Asao Y, Ogura H, Masaki A, Yoshida T, Mori F, Ito A, Yano H, Ri M, Kayukawa S, Kataoka T, Kusumoto S, Ishida T, Hayami Y, Hanamura I, Komatsu H, Inagaki H, Matsuda Y, Ueda R, Iida S.	Global real-time quantitative reverse transcription-polymerase chain reaction detecting proto-oncogenes associated with 14q32 chromosomal translocation as a valuable marker for predicting survival in multiple myeloma.	Leuk Res.	37	1648-55	2013
Nakano N, Kusumoto S, Tanaka Y, Ishida T, Takeuchi S, Takatsuka Y, Akinaga S, Mizokami M, Ueda R, Utsunomiya A.	Reactivation of hepatitis B virus in a patient with adult T-cell leukemia-lymphoma receiving the anti-CC chemokine receptor 4 antibody mogamulizumab.	Hepatol Res.	44(3)	354-7	2014
Mori F, Ishida T, Ito A, Sato F, Masaki A, Narita T, Suzuki S, Yamada T, Takino H, Ri M, Kusumoto S, Komatsu H, Hishizawa M, Imada K, Takaori-Kondo A, Niimi A, Ueda R, Inagaki H, Iida S.	Antitumor effects of bevacizumab in a microenvironment-dependent human adult T-cell leukemia/lymphoma mouse model.	Eur J Haematol.	92(3)	219-28	2014

Miyazaki Y, Fujiwara H, Asai H, Ochi F, Ochi T, Azuma T, Ishida T, Okamoto S, Mineno J, Kuzushima K, Shiku H, Yasukawa M.	Development of a novel redirected T cell-based adoptive immunotherapy targeting human telomerase reverse transcriptase for adult T-cell leukemia.	Blood.	121(24)	4894-901	2013
Kato H, Saito C, Ito E, Furuhashi T, Nishida E, Ishida T, Ueda R, Inagaki H, Morita A.	Bath-PUVA Therapy Decreases Infiltrating CCR4-Expressing Tumor Cells and Regulatory T Cells in Patients With Mycosis Fungoides.	Clin Lymphoma Myeloma Leuk.	13(3)	237-80	2013
Nishikawa H, Sakaguchi S.	Regulatory T cells in cancer immunotherapy	Curr Opin Immunol	27	1-7	2014
Wada H, Isobe M, Kakimi K, Mizote Y, Eikawa S, Sato E, Takigawa N, Kiura K, Tsuji K, Iwatsuki K, Yamasaki M, Miyata H, Matsushita H, Udono H, Seto Y, Yamada K, Nishikawa H, Pan L, Venhaus R, Oka M, Doki Y, Nakayama E.	Vaccination With NY-ESO-1 Overlapping Peptides Mixed With Picibanil OK-432 and Montanide ISA-51 in Patients With Cancers Expressing the NY-ESO-1 Antigen.	J Immunother.	37	84-92	2014
Sugiyama D, Nishikawa H, Maeda Y, Nishioka M, Tanemura A, Katayama I, Ezoe S, Kanakura Y, Sato E, Fukumori Y, Karbach J, Jager E and Shakaguchi S.	Anti-CCR4 mAb selectively depletes effector-type FoxP3^{+}CD4^{+} regulatory T cells, evoking anti-tumor immune responses in humans.	Proc. Natl. Acad Sci USA	110	17945-17950	2013
Atarashi K, Tanoue T, Suda W, Oshima K, Nagano Y, Nishikawa H, Fukuda S, Saito T, Narushima S, Hase K, Kim S, Fritz JV, Wilmes P, Ueha S, Matsushima K, Ohno H, Olle B, Sakaguchi S, Taniguchi T, Morita H, Hattori M and Honda K.	Treg induction by a rationally selected Clostridia cocktail from the human microbiota.	Nature.	500	232-236	2013

Fujiwara S, Wada H, Kawada J, Kawabata R, Takahashi T, Fujita J, Hirao T, Shibata K, Makari Y, Iijima S, Nishikawa H, Jungbluth A, Nakamura Y, Kurokawa Y, Yamasaki M, Miyata H, Nakajima K, Takiguchi S, Nakayama E, Mori M, and Doki Y.	NY-ESO-1 antibody as a novel tumor marker of gastric cancer.	Br J Cancer	108	1119-1125	2013
Liu B, Ohishi K, Orito Y, Nakamori Y, Nishikawa H, Ino K, Suzuki K, Matsumoto T, Masuya M, Hamada H, Mineno J, Ono R, Nosaka T, Shiku H, Katayama N.	Manipulation of human early T lymphopoiesis by coculture on human bone marrow stromal cells: Potential utility for adoptive immunotherapy.	Exp Hematol.	41	367-376	2013
Takino H, Li C, Yamada S, Sato F, Masaki A, Fujiyoshi Y, Hattori H, Inagaki H.	Thymic extranodal marginal zone lymphoma of mucosa-associated lymphoid tissue: a gene methylation study.	Leuk Lymphoma.	54	1742-6	2013
Tamai Y, Hasegawa A, Takamori A, Sasada A, Tanosaki R, Choi I, Utsunomiya A, Eto T, Koh H, Suehiro Y, Kato K, Takemoto S, Okamura J, Uike N, Kannagi M.	Potential contribution of a novel Tax epitope-specific CD4+ T cells to graft-versus-Tax effect in adult T cell leukemia patients after allogeneic hematopoietic stem cell transplantation.	J Immunol	190(8)	4382-92	2013
Ishihara M, Araya N, Sato T, Tatsuguchi A, Saichi N, Utsunomiya A, Nakamura Y, Nakagawa H, Yamano Y, Ueda K.	Preapoptotic protease calpain-2 is frequently suppressed in adult T-cell leukemia.	Blood	121(21)	4340-7	2013
Asanuma S, Yamagishi M, Kawanami K, Nakano K, Sato-Otsubo A, Muto S, Sanada M, Yamochi T, Kobayashi S, Utsunomiya A, Iwanaga M, Yamaguchi K, Uchimaru K, Ogawa S, Watanabe T.	Adult T-cell leukemia cells are characterized by abnormalities of Helios expression that promote T-cell growth.	Cancer Sci	104(8)	1097-106	2013

Kinpara S, Kijiyama M, Takamori A, Hasegawa A, Sasada A, Masuda T, Tanaka Y, Utsunomiya A, Kannagi M.	Interferon-α (IFN-α) suppresses human T-lymphotropic virus type-1 (HTLV-1) gene expression and cell cycling, while IFN-α combined with zidovudine induces p53 signaling and apoptosis in HTLV-1- infected cells.	Retrovirol	10	52	2013
Ando H, Sato T, Tomaru U, Yoshida M, Utsunomiya A, Yamauchi J, Araya N, Yagishita N, Coler-Reilly A, Shimizu Y, Yudo K, Nishioka K, Nakajima T, Jacobson S, Yamano Y.	Positive feedback loop via astrocytes causes chronic inflammation in virus-associated myelopathy.	Brain	136(Pt 9)	2876-87	2013
Sato T, Coler-Reilly A, Utsunomiya A, Araya N, Yagishita N, Ando H, Yamauchi J, Inoue E, Ueno T, Hasegawa Y, Nishioka K, Nakajima T, Jacobson S, Izumo S, Yamano Y.	CSF CXCL10, CXCL9, and neopterin as candidate prognostic biomarkers for HTLV-1-associated myelopathy/tropical spastic paraparesis.	PLoS Negl Trop Dis	7(10)	e2479	2013
Chihara D, Ito H, Matsuda T, Katanoda K, Shibata A, Taniguchi S, Utsunomiya A, Sobue T, Matsuo K.	Association between decreasing trend in the mortality of adult T-cell leukemia/lymphoma and allogeneic hematopoietic stem cell transplants in Japan: Analysis of Japanese vital statistics and Japan Society for Hematopoietic Cell Transplantation (JSHCT).	Blood Cancer J	3	e159	2013
Tsukasaki K, Imaizumi Y, Tokura Y, Ohshima K, Kawai K, Utsunomiya A, Amano M, Watanabe T, Nakamura S, Iwatsuki K, Kamihira S, Yamaguchi K, Shimoyama M.	Meeting report on the possible proposal of an extranodal primary cutaneous variant in the lymphoma type of adult T-cell leukemia-lymphoma.	J Dermatol.	41(1)	26-8	2014
Tokunaga M, Uto H, Oda K, Tokunaga M, Mawatari S, Kumagai K, Haraguchi K, Oketani M, Ido A, Ohnou N, Utsunomiya A, Tsubouchi H.	Influence of human T-lymphotropic virus type 1 coinfection on the development of hepatocellular carcinoma in patients with hepatitis C virus infection.	J Gastroenterol	in press		

III. 研究成果の刊行物・別刷

Clonal evolution of adult T-cell leukemia/lymphoma takes place in the lymph nodes

Akira Umino,[1,2] Masao Nakagawa,[1] Atae Utsunomiya,[3] Kunihiro Tsukasaki,[4] Naoya Taira,[5] Naoyuki Katayama,[2] and Masao Seto[1,6]

[1]Division of Molecular Medicine, Aichi Cancer Center Research Institute, Nagoya, Japan; [2]Hematology and Oncology, Mie University Graduate School of Medicine, Tsu, Japan; [3]Department of Hematology, Imamura Bun-in Hospital, Kamoikeshinmachi, Kagoshima, Japan; [4]Department of Hematology and Molecular Medicine Unit, Atomic Bomb Disease Institute, Nagasaki University Graduate School of Biomedical Sciences, Nagasaki, Japan; [5]Deptment of Internal Medicine, Heartlife Hospital, Okinawa, Japan; and [6]Department of Cancer Genetics, Nagoya University Graduate School of Medicine, Chikusa-ku, Nagoya, Japan

Adult T-cell leukemia/lymphoma (ATLL) is the neoplasm caused by human T-cell leukemia virus type 1 (HTLV-1). We performed oligo-array comparative genomic hybridization (CGH) against paired samples comprising peripheral blood (PB) and lymph node (LN) samples from 13 patients with acute ATLL. We found that the genome profiles of the PB frequently differed from those of the LN samples. The results showed that 9 of 13 cases investigated had a log2 ratio imbalance among chromosomes, and that chromosome imbalances were more frequent in LN samples. Detailed analysis revealed that the imbalances were likely caused by the presence of multiple subclones in the LN samples. Five of 13 cases showed homozygous loss regions in PB samples, which were not found in the LN samples, indicating that tumors in the PB were derived from LN subclones in most cases. Southern blot analysis of TCRγ showed that these multiple subclones originated from a common clone. We concluded that in many ATLL cases, multiple subclones in the LNs originate from a common clone, and that a selected subclone among the LN subclones appears in the PB. (*Blood.* 2011;117(20):5473-5478)

Introduction

Adult T-cell leukemia/lymphoma (ATLL) is the neoplasm caused by human T-cell leukemia virus type 1 (HTLV-1). The disease is associated with poor prognosis due to drug resistance, the occurrence of opportunistic infections, a large tumor burden with multi-organ failure, and hypercalcemia. Shimoyama et al[1] classified ATLL into 4 subtypes: smoldering, chronic, lymphoma, and acute. It is also known that HTLV-1 infection alone does not facilitate the progress of infected $CD4^+$ T cells to fully malignant ATLL cells. Therefore, the search for genes involved in ATLL development and for the specific genes involved in each ATLL type has been actively pursued, albeit with limited success. ATLL-specific chromosomal abnormalities have yet to be found; however, a frequent abnormality found in ATLL is 14q11, which has also been found in other types of T-cell malignancies.[2,3] HTLV-1 provirus integration sites have also been extensively sought, and the sites identified were found to be randomly located. Investigations relying on G-band and fluorescence in situ hybridization analyses have not been fruitful in providing a detailed delineation of the genomic aberrations involved.[4] The use of high-resolution, array-based comparative genomic hybridization (CGH) for comprehensive chromosome analysis should prove useful in the search for genomic aberrations. We showed previously that acute and lymphoma ATLL types possess distinct genomic profiles, as determined by bacterial artificial chromosome array CGH.[5] It should be noted, however, that when lymphoma-type ATLL progresses to manifest more than 2% flower cells in the peripheral blood (PB), it is then classified as the acute type. We set out to analyze the genomic aberrations of acute-type ATLL with paired PB and lymph node (LN) samples in more detail by oligo-array CGH.

An important factor in the diagnosis of ATLL is the identification of monoclonal integration of HTLV-1. It has been reported that the same HTLV-1–infected clone was detected over several years in a chronic-type ATLL patient.[6,7] These types of HTLV-1–infected $CD4^+$ T lymphocytes are believed to accumulate various changes during an extensive latency period of over 50 years.[8] Alterations in genomic copy number represent one example of the type of accumulated genomic changes that can occur. In the present study, we performed high-resolution oligo-array CGH (Agilent Technologies) using a 44 000-probe set against paired samples obtained from the PB and LNs of 13 patients with acute-type ATLL.

Methods

ATLL patients and cell lines

We conducted a survey of genomic profiles by examination of PB and LN samples taken from 13 patients with acute-type ATLL. Paired samples were collected from each patient within 14 days of diagnosis. The PB and LN samples, together with clinical data, were obtained from 13 patients under a protocol approved by the institutional review board of the Aichi Cancer Center. Informed consent was provided according to the Declaration of Helsinki. Patients were diagnosed from those hospitalized between 1988 and 2010 at Imamura-Bunin Hospital and Nagasaki University School of Medicine. The diagnosis of ATLL was based on clinical features, hematologic characteristics, immunophenotype, and the presence of serum antibodies to ATLL-associated antigens. The median age of the patients was

Submitted December 26, 2010; accepted March 11, 2011. Prepublished online as *Blood* First Edition paper, March 29, 2011; DOI 10.1182/blood-2010-12-327791.

The online version of this article contains a data supplement.

The publication costs of this article were defrayed in part by page charge payment. Therefore, and solely to indicate this fact, this article is hereby marked "advertisement" in accordance with 18 USC section 1734.

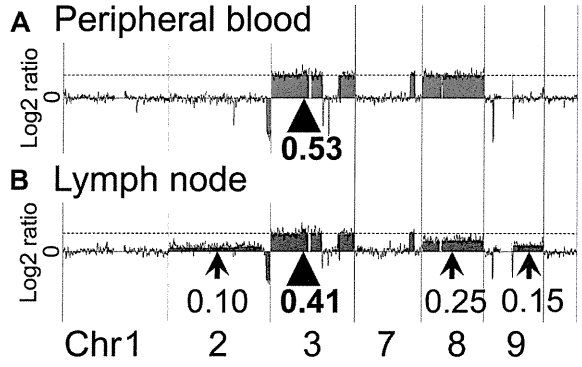

Figure 1. Representative profiles of the PB and LN samples of case 1. Array CGH results for case 1 are shown. (A) In the PB sample of case 1, regions of gain were detected. The log2 ratio of chromosome 3 was 0.53 (arrowhead). The log2 ratios of chromosomes 7 and 8 were the same as for chromosome 3 (dotted line). (B) In the LN sample of case 1, a log2 ratio imbalance was found. Log2 ratios among chromosomes 2, 3, 7, 8, and 9 differed. The log2 ratios of chromosome 3 and 7 were 0.41 (arrowhead and dotted line). Arrows show different log2 ratios: chromosome 2 = 0.10, chromosome 8 = 0.25, and chromosome 9 = 0.15.

57 years (range, 32-74 years). Detailed patient information is provided in supplemental Table 1 (available on the *Blood* Web site; see the Supplemental Materials link at the top of the online article).

Four cell lines, SP-49,[9] HANK1,[10] ATN-1,[11] and Jurkat,[12] were also analyzed. SP-49 is a mantle cell lymphoma cell line, HANK1 is a natural killer/T-cell lymphoma line, ATN-1 is an ATLL cell line, and Jurkat is a T-cell lymphoblast–like cell line.

Peripheral blood samples were obtained from the blood of 8 healthy male donors. PBMCs were isolated by Ficoll-Paque PLUS centrifugation (GE Healthcare).

DNA extraction

$CD4^+$ cells in PB samples were purified using a magnetic-activated cell-sorting protocol (Miltenyi Biotec). High–molecular-weight DNA was extracted from $CD4^+$ cells, frozen LNs, and from the SP-49, HANK1, ATN-1, and Jurkat cell lines using standard proteinase K treatment and phenol-chloroform extraction.[13] Normal DNA was obtained from PBMC samples of 8 healthy male donors.

Oligo-array CGH

Characterization of the genomic aberrations was performed using Agilent 44K Whole Human Genome CGH arrays (Agilent Technologies) containing 44 000 probes. Procedures for DNA digestion, labeling, hybridization, scanning, and data analyses were performed according to the manufacturer's protocol (Agilent Technologies).

CGH data analysis

CGH data were extracted from scanned images using Feature Extraction software (version 10.3; Agilent Technologies). Raw data were transferred to the Genomic Workbench v5.0 software (Agilent Technologies) for further analysis. We defined gains and losses over a continuous 15-probe dataset as a linear log2 ratio average of ≥ 0.05 or ≤ -0.05, respectively, and microdeletion for a range of 3-15 probes as a linear log2 ratio average of ≤ -0.4. A detailed explanation of the log2 ratio is available in the supplemental data. The array CGH data have been deposited in ArrayExpress under the accession number E-MEXP-3042.

Southern blot analysis of HTLV-1 integration and TCRγ rearrangement

Integration of the HTLV-1 provirus genome and TCRγ rearrangement were assayed as described previously.[5,14] In brief, DNA samples (5 μg) of LNs were digested with restriction enzymes (PstI) and electrophoresed through 0.7% agarose gels. The DNA was then transferred onto a Hybond N^+ membrane (Amersham Pharmacia Biotech) and hybridized to randomly primed ^{32}P-labeled DNA probes specific for the HTLV-1 and TCRγ genes. Blots were then washed at the appropriate stringency and visualized by autoradiography. The HTLV-1 probe comprised a 1.0-kb fragment of the pX region, which was PCR amplified using the primers 5′-ccacttcccagggtttggacag-3′ and 5′-tctgcctctttttcgttaaaaagtagagaaatggg-3′, and the TCRγ probe comprised a 0.6-kb fragment of Jγ2.1.[14]

Results

Oligo-array CGH analysis against paired samples obtained from the PB and LNs

In all of the 13 acute-type ATLL cases, genomic aberrations were detected by oligo-array CGH. Representative profiles of the paired samples obtained from the PB and LNs in cases 1 and 2 are shown in Figure 1A and B and Figure 2A and B, respectively.

In the PB sample of case 1, genomic aberration regions showed a constant log2 ratio. Regions of gain were detected on chromosomes 3, 7, and 8. The log2 ratios corresponding to these regions were 0.53, suggesting that there was no imbalance (Figure 1A arrowhead). On the other hand, imbalance of the log2 ratio among chromosomes was found for the LN sample of case 1. Genomic aberrations of the case 1 LN sample were similar to

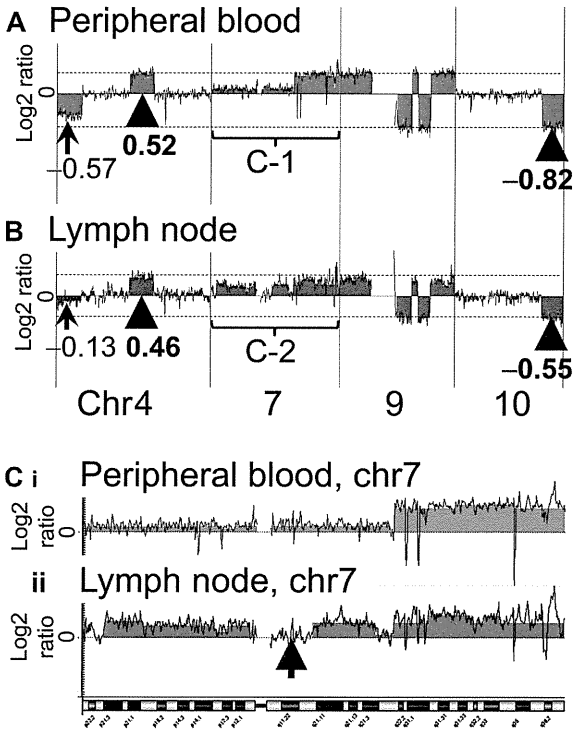

Figure 2. Representative profiles of the PB and LN samples of case 2. The results for case 2 were more complex than those for case 1. In both the PB and the LN samples of case 2, a log2 ratio imbalance was found. (A) In the PB sample, the arrowhead and dotted line indicate the majority of log2 ratios of gain and loss regions. Log2 ratios of the majority of loss regions were −0.82. The log2 ratio of chromosome 4 was −0.57. (B) In the LN sample, the arrowhead and dotted line indicate the majority of log2 ratios of gain and loss regions. Log2 ratios of the majority of loss regions were −0.55. The log2 ratio of chromosome 4 was −0.13. Chromosome 7 regions of PB and LN samples are magnified as Ci and Cii, respectively. (C) Chromosome 7 of the case 2 PB sample shows complex aberrations (i). This result also indicates a log2 ratio imbalance. Chromosome 7 of the case 2 LN sample shows more complex aberrations (ii). An arrow indicates a region (7q11.21-11q.23) without genomic aberration. Ci and Cii suggest that the genomic profiles of the PB and LN samples differ.

Table 1. Array CGH results of paired samples of acute-type ATLL

Case no.	Genome aberrations	Log2 imbalance		Genomic profiles of PB and LN	Common aberration regions between PB and LN	ATLL clones
		PB	LN			
1	+	−	+	different	+	Multiple subclones
2	+	+	+	different	+	Multiple subclones
3	+	−	−	same	+	Monoclone
4	+	+	+	different	+	Multiple subclones
5	+	+	−	different	+	Multiple subclones
6	+	−	−	same	+	Monoclone
7	+	+	+	different	+	Multiple subclones
8	+	−	+	different	+	Multiple subclones
9	+	−	+	different	+	Multiple subclones
10	+	−	+	different	+	Multiple subclones
11	+	−	−	same	+	Monoclone
12	+	−	−	same	+	Monoclone
13	+	+	+	different	+	Multiple subclones
Total	13 (100%)	5 (38.4%)	8 (61.5%)	9 (69.2%)	13 (100%)	9 (69.2%)

+ indicates present; and −, absent.

that of the PB sample. However, the log2 ratios among chromosomes 2, 3, 7, 8, and 9 differed as follows. Regions of gain were detected on chromosomes 2, 3, 7, 8, and 9, as shown by the log2 ratios: chromosome 2 = 0.10, chromosomes 3 and 7 = 0.41, chromosome 8 = 0.25, and chromosome 9 = 0.15 (Figure 1B arrowhead and arrows). The log2 ratio of chromosome 8 was lower than that of chromosomes 3 and 7. Gains of chromosomes 2 and 9 were detected in the LN sample, but not in the PB sample. These results indicated that a log2 ratio imbalance occurred in the LN sample.

Case 2 had a log2 ratio imbalance in both the PB and LN samples (Figure 2A). The genomic aberrations of the case 2 PB sample differed from those of the LN sample, as was also found with case 1. In the case 2 PB sample, regions of loss were detected on chromosomes 4, 9, and 10, as shown by the log2 ratios: chromosome 4 = −0.57 (Figure 2A arrow) and chromosomes 9 and 10 = −0.82 (Figure 2A arrowhead and dotted line). In the case 2 LN sample, regions of loss were also detected on chromosomes 4, 9, and 10, as shown by the log2 ratios: chromosome 4 = −0.13 (Figure 2B arrow) and, chromosomes 9 and 10 = −0.55 (Figure 2B arrowhead and dotted line). These data indicated that both samples had a log2 ratio imbalance. Complex genome aberrations were found for chromosome 7 in the paired samples of case 2. Consecutive gain regions were found in the whole of chromosome 7 of the PB sample (Figure 2Ci, and a region (7q11.21-11q.23) without genomic aberrations was found in chromosome 7 of the LN sample (Figure 2Cii arrow).

A log2 ratio imbalance among chromosomes was present in many other samples of acute-type ATLL, as summarized in Table 1.

Confirmation of log2 ratio imbalance among chromosomes

A log2 ratio imbalance among chromosomes was found in many ATLL clinical samples. We expected that a log2 ratio imbalance would indicate the presence of clones with different genomic aberrations. Therefore, we prepared 2 cell lines, SP-49 and HANK1, which possess different genomic aberrations. The genomic DNA of SP-49 was mixed with that of HANK1. We then conducted oligo-array CGH using the mixed-genomic DNA samples at various ratios.

Array CGH analysis of the SP-49 genome showed some genomic aberration regions, which were consistent with the G-band result that had been reported.[9] Log2 ratios of all 1-copy gain regions were 0.55, and log2 ratios of all 1-copy loss regions were −0.80. Imbalance of the log2 ratio among the chromosomes was not found. The same was true for HANK1, in which genomic aberration regions were consistent with the G-band result that had been reported and an imbalance of the log2 ratio among the chromosomes was not found.[10]

A representative array CGH result using a mixed-DNA sample at a ratio of 7:3 (SP-49:HANK1) is shown in Figure 3. The results showed an imbalance of the log2 ratio among chromosomes. It was possible to reproduce the log2 ratio imbalance. For example, the log2 ratios of chromosomes 2p14-pter, 2q14.3-qter, and 7p were 0.55, 0.15, and 0.46, respectively. These log2 ratios clearly differed. Furthermore, additional regions with different log2 ratios were found.

These results indicated that some of the clones present in the sample that had different genome profiles caused a log2 ratio imbalance in the array CGH result. The log2 ratio did not differ in chromosome 2p, which had a copy region identical to both SP-49 and HANK1.

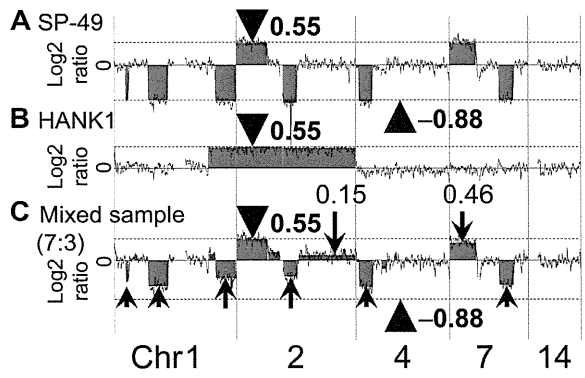

Figure 3. Confirmation of log2 ratio imbalance among chromosomes. The manner in which the log2 ratio imbalance occurred was confirmed. (A) SP-49 showed no imbalance. Log2 ratios of gain regions were 0.55 (arrowhead and dotted line). Log2 ratios of loss regions were −0.88 (arrowhead and dotted line). (B) HANK1 showed no imbalance. Log2 ratios of gain regions were 0.55 (arrowhead and dotted line). (C) Mixed-genomic DNA at a ratio of 7:3 reproduced the log2 ratio imbalance. The log2 ratio of chromosome 2p14-pter of the mixed DNA sample was 0.55 (arrowhead). Chromosome 2p had a copy region identical to both SP-49 and HANK1. Arrows indicate the log2 ratio imbalance.

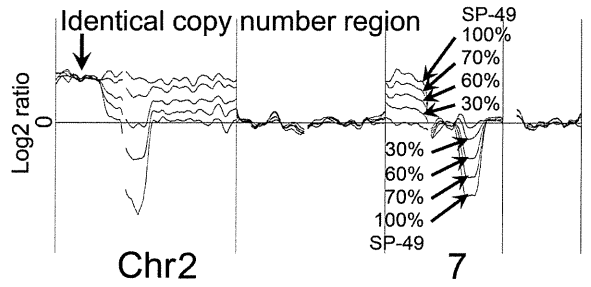

Figure 4. Log2 ratio reflects the ratio of tumor. The genome profiles of mixed-DNA samples comprising various ratios were superimposed. Gain was detected in chromosome 7 of all mixed samples, as shown by the log2 ratio: SP-49 = 0.55; 100%, 7:3 = 0.46; 70%, 6:4 = 0.32; 60%, 3:7 = 0.20; 30%. Loss was also detected in chromosome 7 of all mixed samples as shown by the log2 ratio: Sp-49 = −0.88; 100%, 7:3 = −0.62; 70%, 6:4 = −0.39; 60%, 3:7 = −0.14; 30%. Chromosome 2p had a copy region identical to both SP-49 and HANK1. The log2 ratios never changed in these regions.

Log2 ratios reflect the ratio of tumor

The genome profiles of mixed-DNA samples comprising various ratios were superimposed (Figure 4). The ratios of SP-49 to HANK1 were 7:3, 6:4, and 3:7. These results clearly revealed that the log2 ratio reflected the ratio of the tumor. When tumors included in a sample had identical genomic aberration regions, the log2 ratio never changed in these regions.

Southern blot analysis of HTLV-1 integration and TCRγ rearrangement

HTLV-1 integration

HTLV-1 integration was examined using Southern blot analysis, and the results showed HTLV-1 integration in all of the 11 cases examined. Eight of the 11 cases examined comprised a mono-integration band, whereas the others showed multi-integration bands. (Figure 5A)

TCRγ rearrangement

Southern blot analysis of TCR Jγ rearrangement was also conducted and evaluated as described previously by Moreau et al.[14] The results indicated that all samples were monoclonal (Figure 5B). Five of the 11 cases examined had a 6.8-kb rearrangement band, and 2 had a 2.9-kb rearrangement band. The others showed loss of germinal bands. In case 2, one allele of TCRγ was rearranged, because the germinal band of 8.0 kb was weaker than that of 4.9 kb. Case 7 lost all germinal bands, such as ATN-1, which is an ATLL cell line. This result indicated that both alleles of TCRγ were rearranged at Jγ2.3, because no deletion was found in case 7 by array CGH. Given that 3 or more TCR rearrangement bands were not found, no cases showed definite multi-clonality in tumor cells. These results indicated that the acute-type ATLL examined represented a monoclonal tumor comprising TCR rearrangements and with some possessing multiple integrations of HTLV-1.

Appearance of LN subclones before PB subclones

Array CGH analysis revealed that PB samples from 5 of 13 cases had homozygous loss regions that were not found in the corresponding LN samples of each case. In case 2, 1p12-1p13.1 of the PB sample was seen to represent homozygous loss, unlike the case with the LN sample (Figure 6). However, log2 ratios of same region in the LN sample seemed to be slightly lower than those of neighboring regions. This raised the possibility that a minor

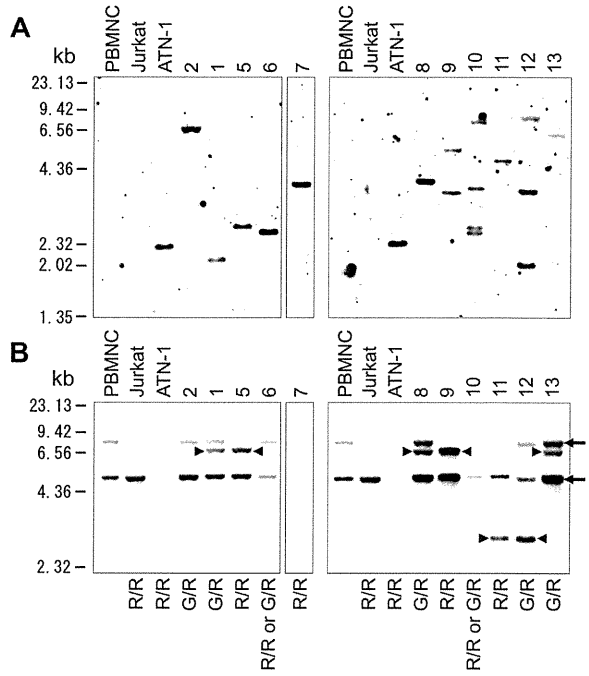

Figure 5. Southern blot analysis. (A) Southern blot analysis of HTLV-1 integration in 11 of 13 cases. (B) Southern blot analysis of TCRγ rearrangement. Arrows indicate the 8.00- and 4.9-kb germline bands. Arrowheads indicate the 6.8- and 2.9-kb rearrangement bands. G indicates a germinal allele; R, rearrangement allele; G/R, rearrangement of one allele; R/R, rearrangement of both alleles.

subclone was present. The PB samples from cases 1, 4, 8, and 10 also had homozygous loss regions that were not clearly found in the corresponding LN samples (Table 2).

No cases had a homozygous loss region in the LN samples when the PB samples had a heterozygous loss in the same regions. Array CGH and Southern blotting results indicated that multiple subclones had developed from one clone. Therefore, when 2 clones were found in a patient, the clone with homozygous loss must have developed from the clone with heterozygous loss. The homozygous loss analysis revealed that in about 40% of ATLL patients, subclones that had appeared in the PB were derived from LN subclones.

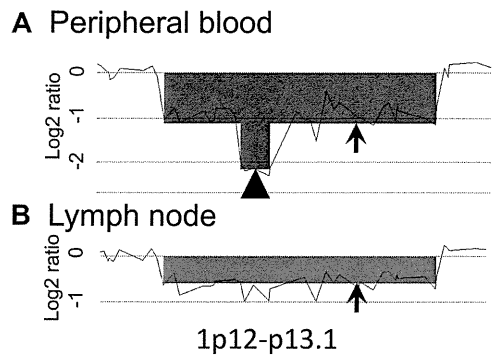

Figure 6. Homozygous loss region analysis. A representative homozygous loss region of case 2 is shown (1p12-p13.1). The total scale of the figure is approximately 2 Mb. The arrowhead indicates a homozygous loss region; arrows indicate heterozygous loss regions. Homozygous loss was found only in the PB sample. The log2 ratio of this region in the LN sample was slightly lower than that in the neighboring regions, suggesting the possibility that a minor subclone may exist in the LNs.

Table 2. PB samples of 5 of 13 cases only had homozygous loss regions that were not found in the LN samples

Case no.	Homozygous loss only in PB	Homozygous loss only in LN	Locus	Gene
1	+	−	3q22.3	*PCCB, STAG1*
2	+	−	1p12-p13.1	*IGSF3*
3	−	−		
4	+	−	6p22.3	*ATXN1*
5	−	−		
6	−	−		
7	−	−		
8	+	−	4q31.21	*INPP4B*
9	−	−		
10	+	−	9q31.2	*KLF4*
11	−	−		
12	−	−		
13	−	−		
Total	5	0		

+ indicates present; and −, absent.

Selected subclone of LNs in the PB

Tumor cells in the PB samples of some cases (eg, cases 1 and 9) appeared to have been selected from multiple subclones. In these cases, a log2 ratio imbalance was not found in the PB sample but was found in the LN sample. This indicated that PB samples were monoclonal and that the LN samples contained multiple subclones. Both samples from each case had common aberrations, and the LN samples had aberrations that were not found in the PB samples. These results may indicate that the LNs contain multiple subclones with different genomic aberrations, and that one of these subclones then appears in the PB (Figure 7).

Discussion

The imbalance and differing genomic profiles of PB and LN samples indicate that acute-type ATLL comprises multiple subclones

In this study, we revealed the presence of a log2 ratio imbalance among chromosomes of LN samples in many patients with acute-type ATLL. Most of the genomic profiles were found to differ from those of the PB samples. Although monoclonal proliferation of acute-type ATLL is referred to in the World Health Organization classification,[15] these data clearly show that acute-type ATLL contains multiple subclones that originate as a result of clonal evolution in ATLL patients.

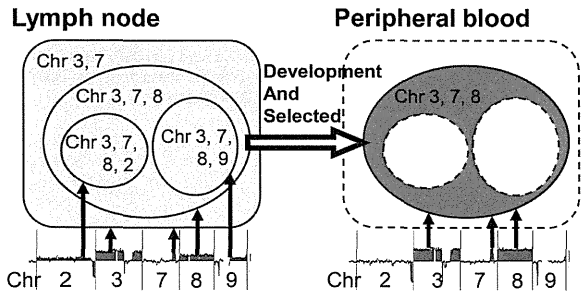

Figure 7. Selected subclone from the LN in the PB. Shown is a schematic representation of a selected subclone from the LN sample in the PB of case 1. In the LN sample of case 1, at least 4 subclones exist: a subclone with chromosome 3 and 7 aberrations; a subclone with additional chromosome 8 aberrations; a subclone with chromosome 3, 7, 8, and 2 aberrations; and a subclone with chromosome 3, 7, 8, and 9 aberrations. Among these subclones, a subclone with chromosome 3, 7, and 8 aberrations appeared in the PB sample.

Shinawi et al[16] reported a case of pediatric AML in which 2 clones with different chromosome aberrations showed a log2 ratio imbalance as detected by array CGH. We were able to reproduce a log2 ratio imbalance among chromosomes by mixing different ratios of DNA prepared from 2 different cell lines. The log2 ratio reflected the ratio of tumor clones. Based on these data, we analyzed the acute-type ATLL data and identified that a log2 ratio imbalance indicated the presence of multiple subclones in a sample. Minority clones with low log2 ratios could be found in this experiment by taking advantage of the high sensitivity associated with the use of array CGH. As a result, the presence of multiple subclones was unambiguously determined.

Cases showing different genomic profiles between PB and LN samples reached as high as 69%. We reported previously that paired samples obtained from different sites had different chromosomal aberrations in some cases.[17] We also reported that sequential samples at chronic and crisis or acute onset and relapse in each case showed different chromosome aberrations or integrations as determined by chromosomal CGH or Southern blot analysis.[17] Similar clonal change has been reported previously in some cases of B-cell lymphoma.[18] Although analysis of sequential samples is important when examining the stability of multiple subclones, it is difficult to acquire sequential samples from acute-type ATLL patients because these patients require immediate chemotherapy. However, chronic-type ATLL can be treated with "watchful waiting," so the clonal stability of ATLL may be explored in these patients.

Our data indicate that acute-type ATLL comprises multiple subclones with differing genomic aberrations. Several morphologic variants of ATLL have been described,[15] and the presence of a mixture of cells of different sizes has been reported. However, the histological type does not correspond to the clinical subtype.[19] Therefore, it is reasonable to postulate that the histological type does not always reflect the clinical features because the tumor subclones may differ at various sites.

HTLV-1 integration and TCRγ rearrangement determined by Southern blotting

We focused on the cell origin of the multiple subclones in each patient. Southern blot analysis revealed a monoclonal band of HTLV-1 integration or monoclonal rearrangement of TCRγ in all samples examined. These data indicated that the ATLL clones in each case had a common tumor cell origin. ATLL research and treatment utilize the Shimoyama classification. Acute-type ATLL represents one subtype in the classification, and is considered to be a monoclonal tumor. Our data are also consistent with this classification. However, it is possible that multiple subclones in the LNs possess a diversity that may account for the variable clinical manifestations and drug resistance that can occur during the treatment of ATLL.

Selection of leukemic clone and diversity in LNs

Array CGH suggested that the subclones in the PB and LNs differed even though they are derived from an identical monoclonal tumor cell, as determined by in Southern blot analysis. Given that the clones are derived from one clone, theoretically the clone with heterozygous loss is never derived from a cell with homozygous loss. Homozygous loss regions were only present in the PB samples examined at a frequency of 38% (5 of 13 cases examined). None of the 5 samples showed homozygous loss

regions found in the LN samples, indicating that in these cases, subclones present in the LNs were not derived from those in the PB. These results suggested that the selected subclones appeared in the PB after subclones developed in the LNs. However, it remains to be determined how these clones in the PB become stable during the course of disease. It is also important to determine whether the tumor cells in the PB can proliferate at the level of tumor cells in the LNs.

In conclusion, the results of the present study showed that there are multiple subclones in acute-type ATLL, all of which possess a common TCR rearrangement and the genomic profiles of which often differ between the PB and LNs. Cases were identified in which a selected subclone from multiple subclones in the LN samples was also identified in the PB samples. ATLL was clinically classified into 4 subtypes by Shimoyama. However, the specific genes that characterize acute-type ATLL have not been identified. Our results reveal that acute-type ATLL is a genetically heterogeneous neoplasm and that clonal evolution of ATLL takes place in the LNs.

Acknowledgments

We thank Dr Koichi Ohshima for diagnoses; Dr Shinobu Tsuzuki, Dr Kennosuke Karube, and Dr Keiichiro Honma for discussions and encouragement throughout this study; and Kyoko Hirano for outstanding technical assistance.

This work was supported in part by grants-in-aid from the Ministry of Health, Labor and Welfare of Japan; from the Ministry of Education, Culture, Sports, Science and Technology of Japan; and from the Japan Society for the Promotion of Science.

Authorship

Contribution: A. Umino performed the experiments, analyzed data, and wrote the paper; M.N. analyzed data and performed experiments; A. Utsunomiya provided advice, discussed clinical data, and treated patients; K.T. provided advice, discussed clinical data, treated patients, and wrote the paper; N.T. analyzed and discussed clinical data; N.K. discussed clinical data; and M.S. supervised the research, discussed clinical data, analyzed data, and wrote the paper.

Conflict-of-interest disclosure: The authors declare no competing financial interests.

Correspondence: Masao Seto, MD, PhD, Division of Molecular Medicine, Aichi Cancer Center Research Institute, 1-1 Kanokoden, Chikusa-ku, Nagoya, Aichi 464-8681, Japan; e-mail: mseto@aichi-cc.jp.

References

1. Shimoyama M. Diagnostic criteria and classification of clinical subtypes of adult T-cell leukaemia-lymphoma. A report from the Lymphoma Study Group (1984-87). *Br J Haematol.* 1991;79(3):428-437.
2. Raimondi SC, Behm FG, Roberson PK, et al. Cytogenetics of childhood T-cell leukemia. *Blood.* 1988;72(5):1560-1566.
3. Shimoyama M, Abe T, Miyamoto K, et al. Chromosome aberrations and clinical features of adult T cell leukemia-lymphoma not associated with human T cell leukemia virus type I. *Blood.* 1987; 69(4):984-989.
4. Maciejewski JP, Tiu RV, O'Keefe C. Application of array-based whole genome scanning technologies as a cytogenetic tool in haematological malignancies. *Br J Haematol.* 2009;146(5):479-488.
5. Oshiro A, Tagawa H, Ohshima K, et al. Identification of subtype-specific genomic alterations in aggressive adult T-cell leukemia/lymphoma. *Blood.* 2006;107(11):4500-4507.
6. Tsukasaki K, Tsushima H, Yamamura M, et al. Integration patterns of HTLV-I provirus in relation to the clinical course of ATL: frequent clonal change at crisis from indolent disease. *Blood.* 1997;89(3):948-956.
7. Etoh K, Tamiya S, Yamaguchi K, et al. Persistent clonal proliferation of human T-lymphotropic virus type I-infected cells in vivo. *Cancer Res.* 1997; 57(21):4862-4867.
8. Okamoto T, Ohno Y, Tsugane S, et al. Multi-step carcinogenesis model for adult T-cell leukemia. *Jpn J Cancer Res.* 1989;80(3):191-195.
9. Daibata M, Takasaki M, Hirose S, et al. Establishment of a new human B cell line carrying t(11;14) chromosome abnormality. *Jpn J Cancer Res.* 1987;78(11):1182-1185.
10. Kagami Y, Nakamura S, Suzuki R, et al. Establishment of an IL-2-dependent cell line derived from 'nasal-type' NK/T-cell lymphoma of CD2+, sCD3-, CD3epsilon+, CD56+ phenotype and associated with the Epstein-Barr virus. *Br J Haematol.* 1998;103(3):669-677.
11. Naoe T, Akao Y, Yamada K, et al. Cytogenetic characterization of a T-cell line, ATN-1, derived from adult T-cell leukemia cells. *Cancer Genet Cytogenet.* 1988;34(1):77-88.
12. Gillis S, Watson J. Biochemical and biological characterization of lymphocyte regulatory molecules. V. Identification of an interleukin 2-producing human leukemia T cell line. *J Exp Med.* 1980;152(6):1709-1719.
13. Seto M, Yamamoto K, Iida S, et al. Gene rearrangement and overexpression of PRAD1 in lymphoid malignancy with t(11;14)(q13;q32) translocation. *Oncogene.* 1992;7(7):1401-1406.
14. Moreau EJ, Langerak AW, van Gastel-Mol EJ, et al. Easy detection of all T cell receptor gamma (TCRG) gene rearrangements by Southern blot analysis: recommendations for optimal results. *Leukemia.* 1999;13(10):1620-1626.
15. Ohshima K, Jaffe ES, Kikuchi M. Adult T-cell leukaemia/lymphoma. In: The National Agency for Research on Cancer, Swerdlow S, Campo E, Lee Harris N, et al, eds. *WHO Classification of Tumours of Haematopoietic and Lymphoid Tissues.* Lyon: World Health Organization; 2008: 281-284.
16. Shinawi M, Erez A, Shardy DL, et al. Syndromic thrombocytopenia and predisposition to acute myelogenous leukemia caused by constitutional microdeletions on chromosome 21q. *Blood.* 2008;112(4):1042-1047.
17. Tsukasaki K, Krebs J, Nagai K, et al. Comparative genomic hybridization analysis in adult T-cell leukemia/lymphoma: correlation with clinical course. *Blood.* 2001;97(12):3875-3881.
18. Siegelman MH, Cleary ML, Warnke R, Sklar J. Frequent biclonality and Ig gene alterations among B cell lymphomas that show multiple histologic forms. *J Exp Med.* 1985;161(4):850-863.
19. Takeshita M, Akamatsu M, Ohshima K, et al. CD30 (Ki-1) expression in adult T-cell leukaemia/lymphoma is associated with distinctive immunohistological and clinical characteristics. *Histopathology.* 1995;26(6):539-546.

Cancer Cell
Article

Polycomb-Mediated Loss of miR-31 Activates NIK-Dependent NF-κB Pathway in Adult T Cell Leukemia and Other Cancers

Makoto Yamagishi,[1,3] Kazumi Nakano,[1] Ariko Miyake,[1] Tadanori Yamochi,[1] Yayoi Kagami,[1] Akihisa Tsutsumi,[1] Yuka Matsuda,[1] Aiko Sato-Otsubo,[4] Satsuki Muto,[1,4] Atae Utsunomiya,[5] Kazunari Yamaguchi,[6] Kaoru Uchimaru,[2] Seishi Ogawa,[4] and Toshiki Watanabe[1,*]
[1]Graduate School of Frontier Sciences
[2]Institute of Medical Science
The University of Tokyo, Tokyo, 108-8639, Japan
[3]Japan Foundation for AIDS Prevention, Tokyo, 101-0061, Japan
[4]Cancer Genomics Project, Graduate School of Medicine, The University of Tokyo, Tokyo, 113-8655, Japan
[5]Department of Haematology, Imamura Hospital, Bun-in, Kagoshima, 890-0064, Japan
[6]Department of Safety Research on Blood and Biologics, NIID, Tokyo, 208-0611, Japan
*Correspondence: tnabe@ims.u-tokyo.ac.jp
DOI 10.1016/j.ccr.2011.12.015

SUMMARY

Constitutive NF-κB activation has causative roles in adult T cell leukemia (ATL) caused by HTLV-1 and other cancers. Here, we report a pathway involving Polycomb-mediated miRNA silencing and NF-κB activation. We determine the miRNA signatures and reveal miR-31 loss in primary ATL cells. MiR-31 negatively regulates the noncanonical NF-κB pathway by targeting NF-κB inducing kinase (NIK). Loss of miR-31 therefore triggers oncogenic signaling. In ATL cells, miR-31 level is epigenetically regulated, and aberrant upregulation of Polycomb proteins contribute to miR-31 downregulation in an epigenetic fashion, leading to activation of NF-κB and apoptosis resistance. Furthermore, this emerging circuit operates in other cancers and receptor-initiated NF-κB cascade. Our findings provide a perspective involving the epigenetic program, inflammatory responses, and oncogenic signaling.

INTRODUCTION

Adult T cell leukemia (ATL) is an aggressive T cell neoplasm with very poor prognosis (Yamaguchi and Watanabe, 2002). Human T cell leukemia virus type I (HTLV-I) is recognized as an etiological factor in T cell malignancy. Although mounting molecular evidence has contributed to our ability to cure several cancers and other diseases, the genetic background of ATL leukemogenesis is not yet fully understood. Thus, it is an urgent request to clarify the molecular mechanism of ATL development.

Constitutive activation of nuclear factor-κB (NF-κB) is observed in the ATL cell lines and primary isolated tumor cells from ATL patients, although the viral oncoprotein Tax, a powerful activator of NF-κB, is not expressed in these malignant cells (Hironaka et al., 2004; Watanabe et al., 2005). NF-κB activation aberrantly contributes to cell propagation and anti-apoptotic responses in ATL and other cancers (Prasad et al., 2010). In our previous study, inhibition of NF-κB activity with a specific inhibitor, DHMEQ, drastically impaired the levels of ATL cell growth and resistance to apoptosis (Watanabe et al., 2005), suggesting that the molecular background of aberrant NF-κB activation may give us potential therapeutic targets. A recent report provided a new readout that NF-κB-inducing kinase (NIK) has a causal role in tumor progression and the aggressive phenotypes of various cancers, including ATL (Saitoh et al., 2008). NIK plays a pivotal role in the noncanonical (alternative) NF-κB pathway as a crucial kinase in receptor-initiating signaling, including signaling from CD40, LTBR, and BAFFR.

Significance

Here, we propose a molecular perspective of the onset of oncogenic signaling. NIK overexpression is a major driving force for constitutive NF-κB activation in various types of cancers. Using ATL cells as a model of NF-κB-addiction, we identified miR-31 as a suppressor of NIK that is completely silenced in ATL cells. Furthermore, an oncogenic function of a subset of Polycomb is implicated in NF-κB signaling via miRNA regulation. This study introduces a fundamental link between the Polycomb-mediated epigenetic regulation and the NF-κB signaling, allowing us to attribute the constitutive activation of NF-κB to epigenetic reprogramming.

Several studies have recently implicated another functional significance of NIK protein in epithelial cell proliferation, inflammatory response, and oncogenic signaling (for review, see Thu and Richmond, 2010). Although the expression level of NIK is strictly maintained by proteasomal degradation in normal cells (Liao et al., 2004), increased level of NIK transcript are observed in some cancers, causing inappropriate accumulation of NIK protein without stimuli (Annunziata et al., 2007; Saitoh et al., 2008). Overexpression of NIK leads to aberrant phenotypes in several cell types; however, little is known about the abnormal accumulation of NIK in malignant cells.

Recent advances have led to deeper understanding of a new aspect of posttranscriptional gene regulation, i.e., regulation by a class of noncoding RNAs. MicroRNAs (miRNAs) are functional RNAs with 18–25 nt in length that contribute to a class of cellular functions by negatively controlling targeted gene expression via base-pairing to 3′ untranslated region (3′ UTR). A single miRNA regulates the expression of multiple genes, and the functions of miRNAs therefore need to be orchestrated for cellular homeostasis (Ventura and Jacks, 2009). In the context of cancer pathology, many studies have provided evidences that miRNAs can act as either oncogenes or tumor suppressors. Although the relationship between miRNA deregulation and oncogenes has been clarified in several cancer cells, there has been no integrated analysis of gene expression in ATL. Since miRNAs have important functions in living cells, miRNA expression needs to be tightly regulated. Our knowledge about the regulatory mechanisms of miRNA expression is very inadequate because research effort has focused mainly on the role of miRNAs, which remains one of the most intriguing questions. miRNA regulation involves multiple steps. miRNA maturation has been identified as an important step, and its deregulation leads to progression and development of cancer (Davis et al., 2008; Trabucchi et al., 2009). Genetic deletion in cancer cells has also been reported to account for specific miRNA defect (Varambally et al., 2008). In addition, miRNA expression seems to be epigenetically programmed. DNA methylation and histone modification are strong candidates for miRNA regulation and their abnormalities, therefore, have causal roles in cancer initiation, development, and progression. In particular, Polycomb group proteins have central functions in cellular development and regeneration by controlling histone methylation, especially at histone H3 Lys27 (H3K27), which induces chromatin compaction (Simon and Kingston, 2009). Recent studies have revealed that the amount of Polycomb family is closely associated with cancer phenotypes and malignancy in breast cancer, prostate cancer, and other neoplasms (Sparmann and van Lohuizen, 2006). However, the substantial status of Polycomb family and their epigenetic impact in ATL cells have not been documented. Furthermore, the general roles of Polycomb proteins in miRNA regulation are mostly unknown. As described above, since miRNAs are multifunctional molecules in gene regulation, it is of pivotal importance to clarify the miRNAs functions and their regulatory circuit in order to formulate therapeutic strategies.

In the present study, we first performed global miRNA and mRNA profilings of the ATL cells derived from patients to precisely define the significance of miRNA expressions and functions.

RESULTS

miRNA Expression Signature in Primary ATL Cells

To characterize the miRNA expression signature in the primary ATL cells, we first performed an miRNA expression microarray analysis. For results with physiological significance, we used total RNA prepared from clinical ATL samples (n = 40, Table S1 available online) and control CD4+ T cells from healthy donors (n = 22) aged 50–70 years. A strict threshold ($p < 1 \times 10^{-5}$) and two-dimensional hierarchical clustering analysis revealed 61 miRNAs that showed significantly altered levels of expression in ATL cells compared with those of control CD4+ T cells (Figure 1A). It is noteworthy that 59 miRNAs out of 61 (96.7%) showed decreased expression in the primary ATL cells. Among them, we identified miR-31 as one of the most profoundly repressed miRNAs in all ATL individuals (fold change, 0.00403; Figure 1B). miR-31 was recently reported as a tumor suppressor and/or metastasis-associated miRNA in metastatic breast cancer. However, the biological functions of miR-31 in lymphocytes have not been studied. We therefore focused on the biological significance and regulatory mechanisms of miR-31 expression in T cells as well as in solid cancers.

miR-31 Negatively Regulates NF-κB Signaling via NIK Expression

To study the functional significance of miR-31 loss, we attempted to identify the target genes of miR-31 using four computational algorithms. We also performed gene expression microarray analysis of the primary ATL cells (n = 52, Table S1) and normal CD4+ T cells (n = 21) in order to detect aberrations in gene expression. Selected putative target genes are known to be involved in cell-cycle regulation and T cell development (Table S2). To experimentally identify the target genes, we performed reporter-based screens as described below. Luciferase-3′ UTR reporter assays demonstrated a remarkable negative effect against upstream gene expression by the *MAP3K14* 3′ UTR sequence (Figure S1B), which is consistent with an initial cloning report (Malinin et al., 1997). MAP3K14, also known as NIK, has a central role in noncanonical NF-κB signaling by phosphorylation of IKKα. A previous report (Saitoh et al., 2008) and the present results (Table S2) show that NIK is overexpressed in ATL cells, leading to constitutive NF-κB activation. As shown in Figure 2A, treatment with a miR-31 inhibitor increased *NIK* 3′ UTR reporter activity, suggesting the involvement of endogenous miR-31 in NIK downregulation. A computational search predicted one site each of miR-31 and miR-31 antisense (miR-31*) binding sites in the *NIK* 3′ UTR (Figure 2B). To identify the regulatory sequence in 3′ UTR of *NIK*, we established additional two reporters with mutated sequence in each potential seed region (Figure 2C; Figure S1C). Mutant 1, which contains mutated sequence in the miR-31 seed region, partially canceled the negative effect of endogenous miR-31 (Figure S1D) and prevented the effect of Anti-miR-31 treatment (Figure 2D). On the contrary, our results suggest that miR-31* does not participate in NIK regulation. miR-31-mediated reporter regulation was also observed in T cell lines (Figure S1E). To confirm the results, we repeated the experiment to examine whether miR-31 could inhibit NIK expression through seed sequence. We made expression plasmid vectors carrying NIK, NIK-3′

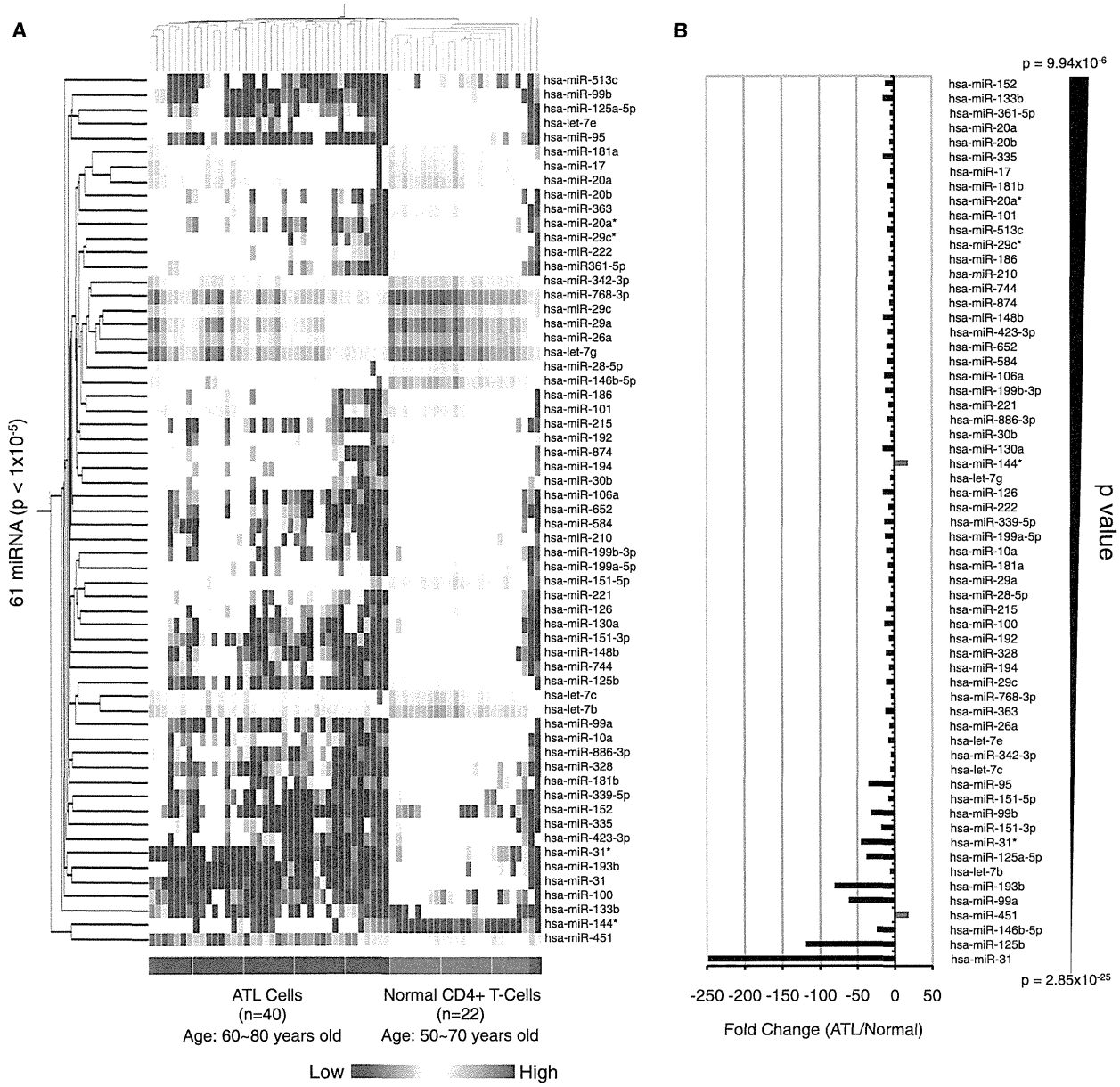

Figure 1. Global Profiling of Cellular miRNA on Primary ATL Cells

(A) Two-dimensional hierarchical clustering analysis and Pearson correlation as similarity measure on the miRNAs expressed at significantly different levels between the ATL (n = 40) and the control (n = 22) groups. Sixty-one miRNAs were identified ($p < 1 \times 10^{-5}$) and by filtering on more than 5-fold changes. A vertical branch shows the expression pattern of the selected miRNAs in each individual.

(B) Fold changes in the 61 miRNAs between ATL and Normal ($p < 10^{-5}$, fold change >5-fold). Selected miRNAs are arranged according to p values. See also Table S1.

UTRWT, or NIK-3′ UTRMu1 and tested their expressions in 293T cells. Results demonstrated that expression of NIK-3′ UTRWT was inhibited by simultaneous introduction of miR-31 (Figure 2E). miR-31 inhibition inversely rescued the NIK level, revealing that the cellular miR-31 level negatively affected that of the NIK protein through its 3′ UTR sequence. These lines of evidence collectively demonstrated that miR-31 recognizes and regulates *NIK* mRNA through specific binding to its 3′ UTR.

Transient introduction of the miR-31 precursor in TL-Om1 cells, which were established from an ATL patient, resulted in downregulation of NIK at the mRNA and protein levels, associated with downregulation of the phospho-IKKα/β level and NF-κB activity (Figures S1F and S1G). In contrast, miR-31 inhibition resulted in accumulation of NIK mRNA and protein in HeLa cells (Figure 2F). Manipulation of the miR-31 level clearly indicated that the miR-31 level negatively correlates with cellular

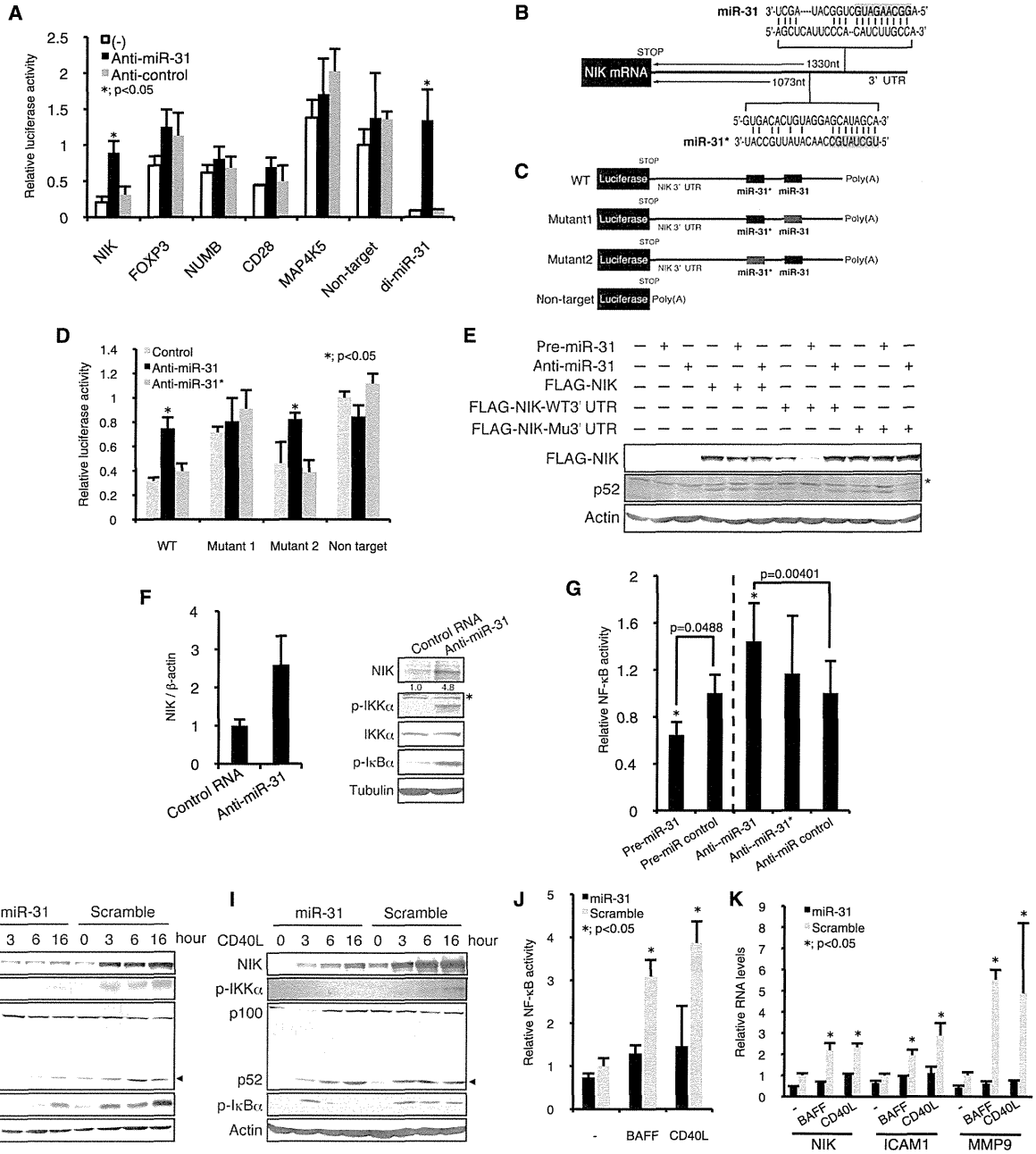

Figure 2. miR-31 Is a Negative Regulator of NF-κB Pathway by Inhibiting NIK Expression

(A) Reporter-based miR-31's target gene screening. A series of 3′ UTR-luciferase reporters was transfected in HeLa cells together with or without miR-31 specific inhibitory RNA (Anti-miR-31) or control RNA (Anti-control). Relative values of Dual-luciferase assay are presented. "Non-target" represents reporter without any 3′ UTR. "di-miR-31" reporter contains two perfect match sequences. The data are presented as mean ± SD of three independent experiments.

(B) Schematic of miR-31 target sites in the *NIK* 3′ UTR.

(C) Mutation-induced reporters. Red box stands for mutated target region (see Figure S1C).

(D) miR-31 negatively regulates *NIK* 3′ UTR analyzed by reporter assay (n = 4, mean ± SD). Luciferase activities of reporter series were tested in a presence or absence of miR-31 inhibitor.

(E) FLAG-tagged NIK protein is negatively regulated through its 3′ UTR and miR-31 binding. Plasmid vectors and miR-31 precursor or miR-31 inhibitor are cotransfected in 293T cells. Western blots showed levels of NIK and endogenous p52. Asterisk indicates nonspecific bands.

(F) NIK mRNA (left) and protein (right) levels in HeLa cells measured by quantitative RT-PCR (n = 3, mean ± SD) and western blotting, respectively. Treatment of miR-31 inhibitor resulted in NIK accumulation. Result of densitometry is shown in the bottom panel. Asterisk indicates nonspecific bands.

(G) Cellular NF-κB activity in HeLa cells (n = 5, mean ± SD) in a presence or absence of miR-31 precursor or inhibitor.

NF-κB activity (Figure 2G). Furthermore, enforced miR-31 expression in B cells attenuated both BAFF and CD40L-mediated NIK accumulation and the subsequent NF-κB signaling (Figures 2H–2K). Consistent with previous reports (Ramakrishnan et al., 2004; Zarnegar et al., 2008b), we also found decreased levels of IκBα phosphorylation. On the other hand, TNF-α-triggered canonical NF-κB activation was not affected by miR-31 in Jurkat cells (Figures S1H–S1K). These results collectively show that miR-31 inhibits the basal and receptor-initiated activities of noncanonical NF-κB pathway. With genetic evidence and an experimental approach, we further demonstrated that the function of miR-31 is well conserved among several classes of species (Figures S1L–S1O). Taking together all these results, miR-31, which is almost completely absent in primary ATL cells, appears to play a critical role in negative regulation of the NF-κB pathway by manipulating the expression of NIK.

miR-31 Suppresses ATL Cell Growth and Promotes Apoptosis by Inhibiting NF-κB

Although it was documented that abnormal NIK accumulation in ATL cells acts as a constitutive activator of the NF-κB pathway, the mechanism underlying overproduction of NIK remains to be elucidated. The results described in the previous section indicated that the amount of miR-31 is linked to the level of NIK, and we therefore speculated that downregulation of miR-31 expression is at least partially responsible for the constitutive activation of NF-κB in ATL cells. Quantitative RT-PCR revealed that *NIK* mRNA levels were negatively correlated with miR-31 levels in primary ATL cell samples (Figure 3A). To investigate the functional roles of NIK and miR-31, we established TL-Om1 cells stably expressing the miR-31 or NIK specific shRNA (shNIK) by retroviral vectors. RT-PCR and western blots showed that expression of miR-31 or shNIK reduced NIK at mRNA and protein levels as well as the levels of phospho-IKKα/β, p52, and IκBα (Figures 3B and 3C). Decreased levels of nuclear RelA and RelB are considered to represent repressed activities of the canonical and noncanonical NF-κB pathways, respectively (Figure 3D). EMSA and NF-κB reporter assays also revealed the repressive function of miR-31 and shNIK on the NF-κB activity (Figures 3E and 3F; Figures S2A, S2B, S5B, and S5C). Re-expression of NIK led to NF-κB activation that was inhibited by miR-31, suggesting a reciprocal relationship between the level of miR-31 and that of NIK.

We and others previously showed that constitutive NF-κB activation is a strong driver of ATL proliferation and prosurvival properties. Here, we examined the effects of miR-31 loss on ATL cell growth. We found that TL-Om1 cells expressing miR-31 or shNIK showed a significant attenuation of cell proliferation compared with control cells. In addition, serum starvation experiments showed greater sensitivity to induced cell death in NIK-repressed cells (Figure 3G). miR-31 expression showed the same phenotypic results in other ATL-derived cell lines (Figures S2C, S2D, and S5E). Jurkat cells do not have significant basal activity of NF-κB, and showed no significant difference in cell growth with or without induced expression of miR-31 (Figure S2E).

Next, we hypothesized that miR-31-mediated NF-κB modulation may affect cellular apoptosis, because numerous studies have demonstrated that NF-κB activation is a strong antiapoptotic factor in ATL and other cancer cells. We found that repression of NIK by miR-31 or shNIK resulted in downregulation of a subset of genes involved in resistance to apoptosis such as BCL-XL, XIAP, and FLIP (Figure 3H), suggesting that miR-31 has a role in proapoptosis through inhibition of NF-κB activity. To assess the biological function of miR-31 in apoptosis signals, we utilized a lentivirus gene transfer system for cell lines and freshly isolated tumor cells. The lentivirus vector is competent to infect nondividing cells and the infected cells can be monitored by the fluorescence of Venus. We found that lentivirus-mediated miR-31 expression promoted basal and Fas-directed apoptosis in TL-Om1 cells (Figure 3I). Venus-negative population showed no significant changes, demonstrating the specificity of miR-31 activity. To confirm the relationship among miR-31, NIK, and NF-κB signaling, we also prepared another retroviral vector encoding NIK without its 3′ UTR sequence. As results, re-expression of NIK reversed the miR-31-mediated apoptosis. In addition, miR-31 expression led to caspase 3 activation (Figure 3J). Collectively, these findings indicate that miR-31 mediates apoptosis through repression of NIK in ATL cell lines.

Tumor cells from ATL patients primarily represent the malignant characteristics. In fact, miR-31 loss is found from patient samples (Figures 1 and 3A). To demonstrate the responsibility of miR-31 for tumor cell survival, we tested whether lentivirus-mediated miR-31 expression has a killing effect against tumor cells. After establishment of lentivirus infection, the apoptotic cells were determined by flow cytometry. The results revealed that expression of miR-31 facilitated tumor cell death. Since NIK repression by shRNA lentivirus also showed a strong killing effect, NIK and NF-κB activity are suggested as crucial players for survival in ATL tumor cells (Figure 3K). Strong toxicities were not observed in normal resting lymphocytes that express low levels of NIK. Taken together, these lines of experimental evidence, including data from cell lines and primary ATL cells, definitively support two notions that (1) miR-31 acts as a tumor suppressor in T cells, and (2) NIK-regulated NF-κB has pivotal importance in cancer cell survival.

Loss of miR-31 Occurs in T Cells with Genetic and Epigenetic Abnormalities

The results described above together with previous publications indicate that regulation of miR-31 expression has profound impacts on multiple functions in human tumors as well as in normal cells. However, little is known about the regulatory mechanism of miR-31 expression. The human gene that encodes miR-31, *hsa-miR-31*, is located at 9p21.3, which is

(H–K) miR-31 attenuates signal-dependent NF-κB activation in B cells. (H and I) BJAB cells expressing miR-31 or control RNA were treated with BAFF (0.2 μg/ml) or CD40L (0.5 μg/ml) for indicated time periods. The protein levels of NIK, phospho-IKKα/β, p100/p52 (arrowheads indicate active p52), and phospho-IκBα were shown. Actin was detected as control. (J) NF-κB activity (n = 5, mean ± SD) evaluated by NF-κB-luciferase reporter assay at 24 hr after cytokine treatments. (K) NF-κB-dependent gene expressions were inhibited by miR-31 (n = 3, mean ± SD). See also Table S2 and Figure S1.

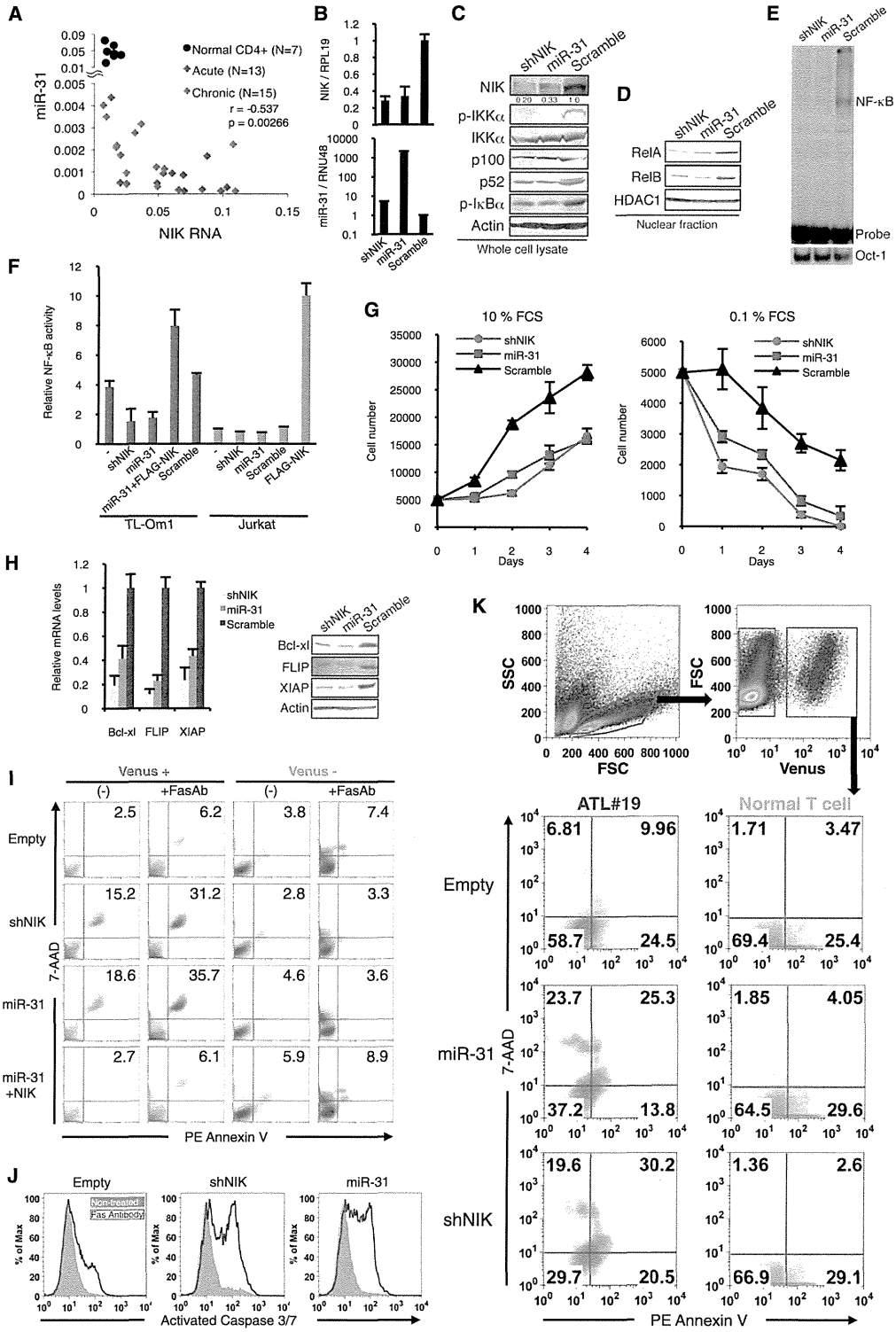

Figure 3. Loss of miR-31 Is Responsible for Constitutive NF-κB Activation, Abnormal Cell Growth, and Resistance to Apoptotic Cell Death in ATL Cells

(A) Expression levels of miR-31 and *NIK* in individual ATL patients and normal controls using data set obtained by quantitative RT-PCR. Pearson's correlation coefficient within ATL samples was described in the graph.

adjacent to clusters of the *CDKN2* and *IFNA* families, and is a well-known hotspot of genomic loss in several types of human cancers. We performed genome-wide scans of genetic lesions in 168 ATL samples and demonstrated that 21 ATL cases (12.5%) had genomic deletion of 9p21.3 containing the *hsa-miR-31* coding region (Figure 4A; Figure S3A). All of these cases also have genomic defect in *CDKN2A* region. A major proportion of ATL cases that are without genetic deletion and somatic mutation in the *hsa-miR-31* region showed remarkable loss of miR-31 expression (Figure 4B). Detailed expression profiling revealed drastic downregulation of *Pri-miR-31* transcription in the primary ATL cells (Figure 4C). There was a strong correlation between the levels of mature miR-31 and primary transcript ($r = 0.9414$, $p = 5.45 \times 10^{-8}$). *hsa-miR-31* is located in intronic region of *LOC554202* gene. However, *LOC554202* mRNA levels were very low in primary T cells and there was no significant difference between ATL and normal cells, strongly suggesting that loss of miR-31 expression is due to specific transcriptional suppression in ATL cells. Using computational analysis, we identified a putative TATA box and transcriptional start site (TSS) 2500 bp upstream of the miR-31 coding region (Figure 4D). Although no CpG islands were found in this region, we unexpectedly discovered an assembly of YY1-binding motifs upstream of the miR-31 region in human and mouse (Figure 4D; Figure S3C). YY1 is a pivotal transcription factor and a recruitor of the Polycomb repressive complex (PRC) (Simon and Kingston, 2009). Convergence of the YY1 binding sequence, especially the repressive motif (Figure S3D), seems to be evolutionarily conserved, suggesting that YY1 is important in the regulation of miR-31 transcription. We further performed chromatin immunoprecipitation (ChIP) to evaluate repressive histone hallmarks, including di- and trimethylated H3K9 (H3K9me2 and H3K9me3) and trimethylated H3K27 (H3K27me3). The results showed higher levels of methylation at H3K9 and H3K27 in a broad area containing the miR-31 coding region (Figure 4E). As shown in Figures S3E–S3G, there was an inverse correlation between the levels of miR-31 expression and repressive histone methylation. These data allowed us to hypothesize that histone methylation, especially that of Polycomb family-dependent H3K27me3, may contribute to miR-31 repression. To confirm our hypothesis, we performed a YY1 knockdown experiment using a specific shRNA (Figures 4F–4I). As expected, knockdown of YY1 led to an increase in the levels of *Pri-miR-31* and mature miR-31 (Figures 4F and 4G). Furthermore, ChIP assays showed that YY1 occupied the miR-31 region, especially in the upstream region of TSS, where there is an array of YY1 binding sites (Figures 4D and 4H). The results also demonstrated that decreased occupancy of YY1 and concomitant derecruitment of EZH2, a key component of PRC2, were induced by YY1 knockdown, indicating involvement of EZH2 in the repressive complex recruited to the miR-31 region (Figures 4H and 4I; Figure S3H). These results collectively suggest that YY1 regulates PRC2 localization and initiates miR-31 suppression. Indeed, we found significant escalation of methylated histone H3K9 and H3K27 at the miR-31 locus of peripheral blood lymphocytes of ATL patients (Figure 4J), indicating that aberrant abundance of suppressive histone methylation may be responsible for the loss of miR-31 in the primary ATL cells.

Overexpression of PRC2 Components Leads to miR-31 Repression

Given that Polycomb-mediated repressiveness affects miR-31 level, our findings imply that the amount of EZH2 is related to miR-31 expression (Figure 4I; Figures S3G and S4A). We found a significantly upregulated expression of PRC2 components, especially EZH2 and SUZ12, in the primary ATL cells (Figures 5A and 5B; Table S3). Quantitative RT-PCR revealed that miR-31 levels inversely correlated with both *EZH2* and *SUZ12*, respectively (Figure 5C). miR-101 and miR-26a, which are putative negative regulators of EZH2, seem to be associated with this relationship in ATL cells (Figures S4B–S4E). To further confirm our hypothetical mechanism linking the epigenetic machinery and miR-31 expression, we performed a "loss-of-PRC2-function" assay. Retroviral delivery of shSUZ12 and shEZH2 in the ATL cell lines resulted in a great increase in the levels of *Pri-miR-31* and its mature form (Figure 5D; Figure S4F). Knockdown of PRC2 induced histone demethylation at H3K27 in the miR-31 region, which is concomitant with the decrease in H3K9me3 levels, EZH2 occupancy, and HDAC1 recruitment (Figure 5E), suggesting that this multimeric complex leads to a completely closed chromatin architecture as a result of histone modifications in the miR-31 genomic region.

To further examine whether the proposed mechanism holds true in other human cancers, we analyzed a couple of carcinoma cell lines, including HeLa cells and nonmetastatic and metastatic breast carcinoma cell lines, MCF7 and MDA-MB-453 cells, respectively. qRT-PCR revealed that expression of *EZH2* and *SUZ12* inversely correlated with miR-31 levels (Figure S4G).

(B) miR-31 restoration by retroviral vector inhibits *NIK* RNA accumulation in TL-Om1 cells. The results of *NIK* and mature miR-31 quantifications are shown (n = 3, mean ± SD).
(C) miR-31 or shNIK expression downregulates NIK protein expression and inhibits downstream pathway of noncanonical NF-κB in TL-Om1 cells.
(D) Reduced nuclear translocation of RelA and RelB proteins in miR-31- or shNIK-expressing TL-Om1 cells.
(E) miR-31-dependent downregulation of NF-κB activity in TL-Om1 cells examined by EMSA.
(F) NF-κB-luciferase reporter assays (n = 5, mean ± SD). FLAG-NIK plasmid was transiently introduced 48 hr prior to the assay.
(G) miR-31 level is relevant to proliferation of ATL cells. Cell proliferation curve of TL-Om1 cells were evaluated in two FCS conditions (n = 3, mean ± SD).
(H) Apoptosis-related gene expression in TL-Om1 cells analyzed by qRT-PCR (n = 3, mean ± SD) and western blots.
(I) Lentivirus-mediated NIK depletion promotes basal and Fas antibody-mediated apoptosis. Venus-positive population represented lentivirus-infected cells. Apoptotic cells were determined by PE-Annexin V / 7-AAD stainings (n = 4). Representative FACS analyses are shown.
(J) miR-31 activates Caspase 3/7 determined by FACS (n = 3).
(K) miR-31 expression and NIK depletion induce tumor cell death. Primary tumor cell from ATL patient and healthy CD3+ T cells were infected with lentivirus and analyzed by FACS. The apoptotic cells were defined by sequential gating beginning with FSC-SSC to select intact lymphocytes, subgating on the Venus-positive population, and calculating the PE-Annexin V and 7-AAD profilings. Representative result is shown and summarized data are presented in Figure 6J. See also Figure S2.